Regenerative Engineering and Translational Medicine (2019) 5:290–296
https://doi.org/10.1007/s40883-019-00108-3

Silicon-Substituted Hydroxyapatite Particles and Response of Adipose Stem Cells In Vitro

M. Eatemad[1] · S. Labbaf[1] · A. Baharlou Houreh[2] · M. H. Nasr Esfahani[2]

Received: 9 December 2018 / Accepted: 2 May 2019 / Published online: 29 May 2019

Abstract

Due to the similarity of synthetic hydroxyapatite (HA) to natural bone tissue, but, because of its low degradation rate, the current study focuses on silicon-substituted HA (Si-HA) synthesis, characterization, and biological evaluations. Si-HA was successfully prepared through sol-gel processing route and characterized using SEM, EDX, XRD, and FTIR. Si-HA particles were found to be non-cytotoxic following exposure to adipose stem cells (ADSCs). In fact, Si-HA particles showed a high level of matrix mineralization following prolonged and continuous exposure to ADSCs. It is suggested that the incorporation of Si in HA structure positively affects cellular behavior, associated with a higher degradation rate, and subsequently greater level of ionic product release from Si-HA particles.

Lay Summary

Hydroxyapatite (HA) has long been applied as bone substitutes but its low degradation rate limits its application. One approach is the incorporation of silicon (Si) within HA structure. This study confirms that Si-substituted HA enhance stem cell proliferation and promote osteogenic differentiation. Hence, Si-HA could be utilized in composites, scaffolds, and coatings for bone-related disorders.

Keywords Si-HA particles · Bone tissue engineering · Adipose stem cells

Introduction

Bone is a natural organic–inorganic nanocomposite consisting of mineral phase hydroxyapatite (HA) embedded within collagen fibrils [1]. Synthetic HA is chemically similar to the inorganic component of bone matrix—a very complex tissue with general formula of $Ca_{10}(OH)_2(PO_4)_6$ [2, 3]. The close chemical similarity of HA to natural bone has led to extensive research efforts to use synthetic HA as an ideal alternative for orthopedic applications in the form of fillers, coatings, and bone-regenerating scaffolds [2, 4–8]. The main advantage of synthetic HA is its biocompatibility and good osteoconductive and osteoinductive capabilities [4–10]. However, one main drawback of the use of HA in bone-related applications is their low degradation and as a result lower bioactivity compared to bioactive glasses of various compositions [11, 12]. Recently, there has been great effort in introducing various ions into HA lattice.

It has been reported that the substitution of certain ions in HA structure have led to improved bioactivity compared to pure HA. One element of interest is silicon (Si), which has shown to induce a higher dissolution rate and stimulates osteoblast activity in vitro compared to pure HA [13, 14]. Si is one of the trace elements known to be essential for biological processes. Previously, aqueous Si has shown to induce precipitation of HA in bone tissue through the stimulation of bone ingrowth as a calcifying agent [15]. Hence, the incorporation of Si in HA lattice is considered to be a potential method for improving the bioactivity of HA [16, 17]. In Si-HA structure, a small percentage of the phosphate ions (PO_4^{-3}) are replaced by silicate ions (SiO_4^{-4}).

Several attempts have been made to prepare Si-HA by a variety of synthesis routes including sol-gel, solid-state reactions, and hydrothermal and precipitation methods

✉ S. Labbaf
s.labbaf@cc.iut.ac.ir

[1] Department of Materials Engineering, Isfahan University of Technology, Isfahan 84156-83111, Iran

[2] Department of Cellular Biotechnology, Cell Science Research Center, Royan Institute for Biotechnology, ACECR, Isfahan, Iran

[18]. Amongst all methods applied for the synthesis of Si-HA, sol-gel is often a preferred method due to the production of materials with higher crystallinity and the proportion of calcium to phosphorus close to the stoichiometry [19–22].

Numerous approaches that stimulate bone healing are becoming more advanced, due to the increase in life expectancy and worldwide aging population. There have been limited studies on the potential of synthetic HA in osteogenic differentiation of stem cells. Therefore, the main aim of the current study was to examine the response of adipose stem cell (ADSCs) to HA and Si-HA. ADSC can easily be isolated from adipose tissue and have shown great ability to differentiate in vitro towards osteogenic, adipogenic, myogenic, and chondrogenic lineages [23–28]. The aim of the current study is to prepare and characterize Si-HA particles and evaluate the biological properties of the obtained structure to confirm their suitability in bone regeneration applications.

Materials and Method

Synthesis of Si-HA Particles

The quantities of the reactants were based on the assumption that silicate is substituted by phosphate in the HA lattice. On this assumption, the following molar ratio of Ca/(P + Si) = 1.67 was applied. Briefly, 7.85 ml (8.39 g) triethyl phosphate (TEP) was hydrolyzed in 4.38 ml water for 24 h. Then, 3.08 ml (2.86 g) tetraethyl orthosilicate (TEOS) was added followed by 18.8 g of $Ca(NO_3)_2 .4H_2O$. Stirring was continued for 3 h to achieve a homogeneous solution. Then, the gel was heated at 60 °C for 48 h to stabilize the gel. Then, the gel was dried at 120 °C for 24 h and white powder created. This dried powder was sintered at 900 °C for 2 h. The obtained particles were then ball milled [10].

Characterization Techniques

X-ray Diffraction (XRD)

The crystalline phases of powders heat-treated to 900 °C were investigated with XRD over a range of 5–70 2 . Powder XRD scans were performed using a Phillips PW1050 diffractometer (PANalytical, NL) with monochromatic Cu Ka X-rays, and operated at 40 kv and 40 mA, a 0.05 step size and a rate of 2.5 at 1 S. Phillips HIGHSCORE PLUS software was used to identify phases in the heat-treated CaP powders. ICDD (International Centre for Diffraction Data) powder diffraction files of HA (09-0432), TEP, TCP, Ca (NO3), TEOS were compared to observed diffraction patterns.

The values of full width at half-maximum (FWHM) of the peak of the (002) plane, representative of the crystallites along the c-axis and of the peak of the (300) plane, and

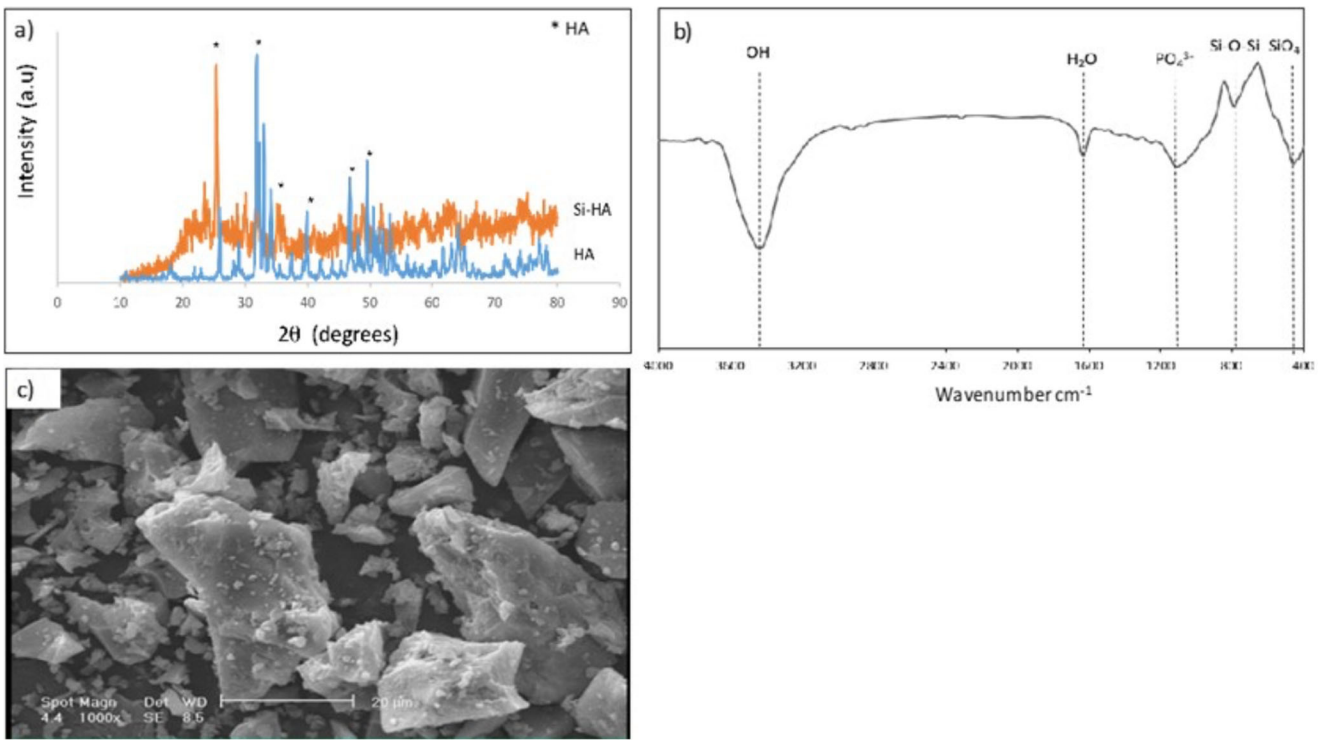

Fig. 1 **a** XRD. **b** FTIR. **c** SEM of Si-HA powder

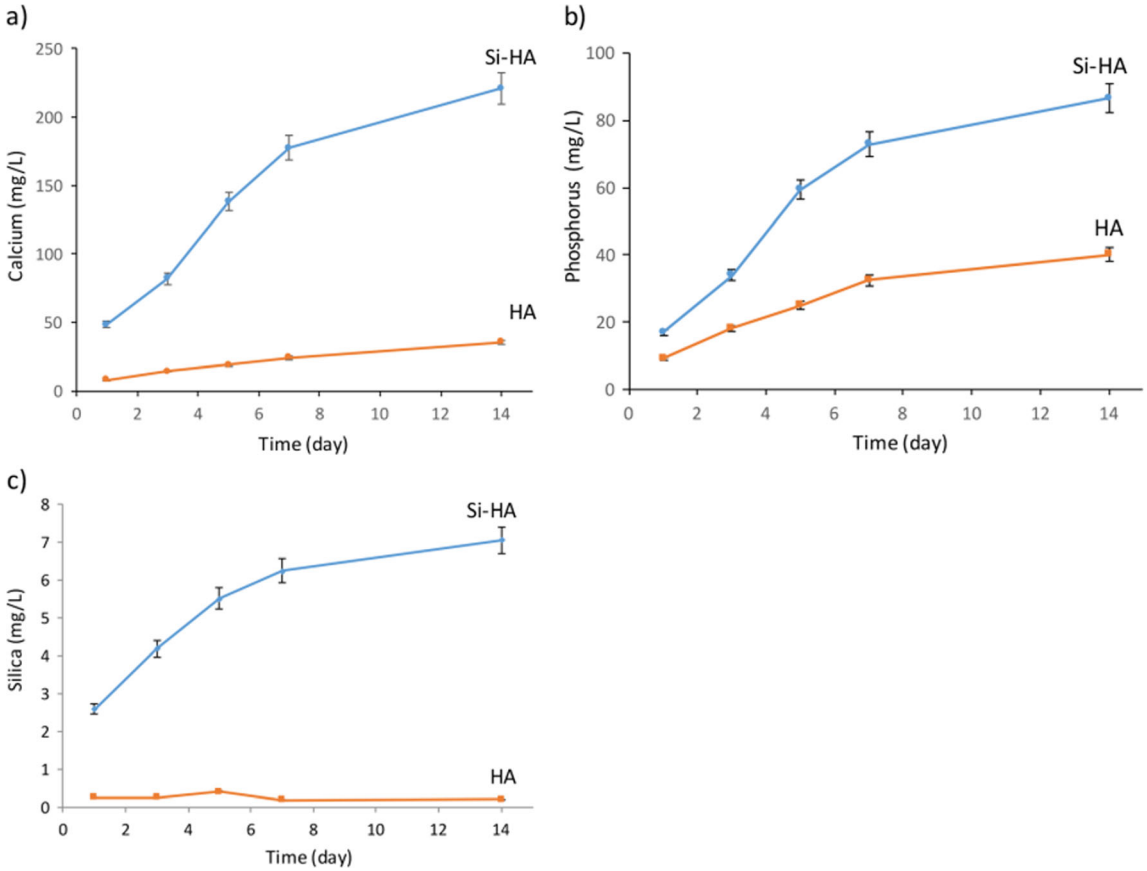

Fig. 2 Dissolution profiles for HA and Si-HA after immersion in DMEM for 14 days

representative of the crystallites along the a-axis were used in the calculation according to the Scherrer's equation (1):

$$D = k\,\lambda/\beta\,\cos\theta \quad (1)$$

where D is the crystallite size in Å, k is Scherer constant (0.89), λ is the wavelength of X-rays beam (1.5406 Å), θ is the diffraction angle, and β is defined as the diffraction FWHW, expressed in radians. Determination of the lattice constants of HA and Si-HA was made by refinement of XRD data of samples calcined at 900°C using FullProf Suite software program.

Scanning Electron Microscopy

A Philips XL30 scanning electron microscope (SEM) equipped with an energy-dispersive X-ray analysis was used to study morphology Si-HA samples. Before observation, the surface of each sample was coated with a thin layer of gold.

Fourier-Transform Infrared Spectroscopy

For further structural and compositional investigations, Fourier-transform infrared spectroscopy (FTIR) spectroscopy was employed running in transmission mode using KBr pallets. Scans were taken over the range of 400 to 4000 cm^{-1}.

Ionic Release Study

Degradation of HA and Si-HA was conducted in high glucose Dulbecco's modified Eagle's medium (DMEM) following 1, 3, 5, 7, and 14 days in accordance with previous studies [29, 30]. At the end of each time point, medium was removed and the solution was filtered and examined by inductive coupled plasma optical emission spectroscopy (ICP-OES Perkin Elmer Optima 7300 DV, USA).

Cell Study

Isolation and Cell Culture of ADSCs

ADSCs were extracted from human buccal fat pads (BFPs) as previously described by Beigi et al. and kept in growth medium containing high glucose DMEM supplemented with 15% FBS, 1% L glutamine (Gibco), 100 U/ml penicillin, 50 μg/ml streptomycin, and 0.25 μg/ml amphotericin B. Cells were subcultured at confluence, and all experiments were carried in passages 4 to 5 [26].

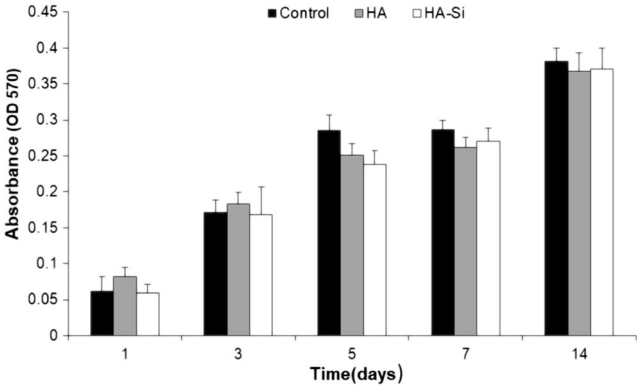

Fig. 3 Cytotoxicity assays using Alamar blue following exposure of 600 μg/ml HA and HA-Si powders. Values represent the mean SD of two individual experiments each performed in triplicate. Data are normalized relative to control of day 1

Powder Exposure to ADSCs

ADSCs were seeded in a 24-well plate at a seeding density of 5000 cells/cm^2 and incubated for 24 h to allow cell attachment. The cell medium was supplemented with 10% fetal bovine serum, 1% L-glutamine, 1% penicillin-streptomycin, and 1% non-essential amino acid. HA and HA-Si powders were tested at a concentration of 600 μg/ml. Following UV sterilization, the powder at a given concentration was transferred into a cell culture insert as previously described [30] (Millicell® Hydrophilic PTFE, pore size of 0.4 μm) and placed in a 24-well plate containing ADSCs.

Cell Viability

Alamar blue cytotoxicity/proliferation assay (Invitrogen, UK) was performed according to the manufacturer's protocol to determine whether HA and HA-Si powders were cytotoxic. Briefly, ADSCs were seeded in a 24-well plate at a seeding density of 5000 cells/cm^2 and incubated for 24 h to allow cell attachment. At the end of each time point, insert and medium were removed and 500 μl of Alamar blue solution (1:10 culture medium: Alamar blue reagent) was added to each well and incubated for 2 h. Optical density was measured at 570 nm using the microplate spectrophotometer multi-well plate reader (Bio-Rad, USA). The results represent the mean values ± SD of two individual experiments each performed in quadruplicate.

Matrix Mineralization

Alizarin red staining was applied to determine the presence of extracellular matrix mineralization following 21-day post seeding. The ADSCs were seeded at 5000 cells/cm^2 in a 24-well plate and cultured in the presence of HA and HA-Si powders up to 21 days and the medium was changed every 3 days. At the end of 21 days of culture, cells were washed with PBS and fixed with methanol for 10 min at room temperature. Five hundred microliters of the prepared alizarin red solution (dissolve 2 g of alizarin red in 100 ml distilled water, pH adjustment to 4.1–4.3 with 0.1% NH_4OH) was added to each well for 20 min. The dye was then drained and the cells were washed extensively with distilled water and viewed under a light microscope (Olympus CKX41SF, Philippines).

For Alizarin red quantification, at the end of 21 days of culture, cells were washed with PBS and were fixed in 96% ethanol for 15 min at room temperature, then stained with 0.2% alizarin red solution in water (pH 6.4) at room temperature for 1 h. Alizarin red was dissolved in a solution of 20%

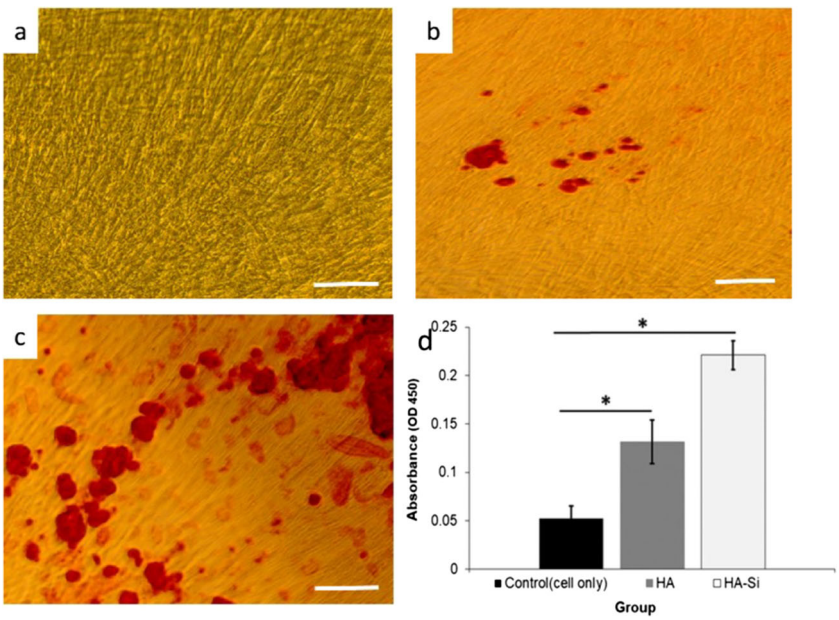

Fig. 4 Alizarin red staining of mineralized nodules of ADSCs cultured in the presence of **a** BM (control) 600 μg/ml of **b** HA and **c** Si-HA tested on day 21, in the absence of osteogenic supplements. Scale bar 100 μm. **d** Normalized alizarin red staining absorbance at 21 days post seeding in different groups. (*) indicates the statistical significant difference (*$p < 0.05$ relative to control)

methanol and 10% acetic acid in water for 15 min. Liquid was then transferred to a 96-well plate and read on a spectrophotometer at a wavelength of 450 nm using the microplate spectrophotometer multi-well plate reader (Awareness Technology Stat Fax 2100 Microplate Reader, USA) [31].

Results and Discussions

Figure 1 a represents XRD patterns for both HA and Si-HA powders. In the XRD pattern for Si-HA, broad peaks corresponding to HA phase are detected but with low crystallinity and absence of any secondary crystalline phases. It is suggested that the low crystallinity is due to the low processing temperature in addition to the substitution of SiO_4^{4-} ion in the HA lattice which limits the crystallization phase [32]. Although XRD patterns effectively correspond to that of pure HA, the diffraction peaks lose intensity with adding silicate. From XRD pattern, it is also evident that there is a slight shift of the Si-HA peaks to a lower Bragg's angle compared to a pure HA at around 25°, which could further suggest the incorporation of Si ions.

Figure 1 b depicts FTIR spectra for Si-HA powder. The strong bands in the range 900–1200 cm^1 correspond to P–O stretching vibration modes of the phosphate groups. The broad band at about 1638 cm^{-1} corresponds to in-plane water bending mode [33, 34]. The band at about 800 cm^{-1} might be assigned to either the silicate group or to the O–Si–O bending [35]. The band at around 490 cm^{-1} is attributed to the presence of $(SiO_4)^{4-}$ groups in the Si-HA structure [19, 36]. Furthermore, the morphology Si-HA is presented in Fig. 1 c, where the particles appear to have a non-uniform irregular structure.

Degradation and hence ionic dissolution of HA and Si-HA were studied in DMEM at various time points. The release profile for Ca, P, and Si was conducted using ICP as shown in Fig. 2. It is evident that the incorporation of Si in HA lattice has had a significant effect on the release of ions in vitro. This find is in good agreement with previous studies [37–40]. The release of Ca is almost 20 times greater in Si-HA than HA following 14 days in culture. Phosphorus release is 3 times higher in Si-HA than pure HA. The three ions of Ca, P, and Si are known as stimulatory ions which have significant effect on cellular behavior in vitro and in vivo [10, 34].

Cellular metabolic activities of ADSCs were studied using Alamar blue assay (Fig. 3). Cells were cultured for 1, 3, 5, 7, and 14 days in medium. At the end of ach time point, cells were tested for cytotoxicity. Overall, there were no significant levels of toxicity between the controls and HA and Si-HA groups tested. In fact, the particles do not influence cellular growth trend. Interestingly, at days 1 and 3, the HA group appears to have a higher proliferation rate than the control but then this decreases on the following days. However, this decrease is not significant. Furthermore, to study the effect of HA and Si-HA on early differentiation of ADSCs, following 21 days in culture, in the absence of osteogenic supplements, Alizarin red staining was applied (Fig.4). Cells treated with HA and Si-HA display mineralized nodules compared to the control group (Fig. 4a–c). It is evident that mineralized nodules cover a great area per field in Si-HA than pure HA. This suggests the great role of Si on cell differentiation [41]. In addition, it is known that the incorporation of Si in HA structure has a profound effect on HA degradation rate which results in the release of PO_4^{3-} as well as Si, as shown in Fig.3. This will ultimately lead to positive effects on cellular behavior in vitro [32, 34, 42].

Figure 4 d shows quantitative analysis of osteogenic differentiation of ADSCs. The HA and Si-HA groups clearly demonstrate a significant level of osteogenic differentiation compared to control group (only cell). This relates to the release of ionic products from HA (Ca and P) and Si-HA (Ca, P, and Si) which greatly contribute to cellular behavior. Silicon has long been known to influence calcification and extracellular matrix formation, and to have a positive effect on osteoblast activity [9, 25]. In addition, both calcium and phosphorus are the main components in bone tissue, so it is believed that the release of these ions from HA would contribute in new bone formation. Phosphate is also known to play a key role in extracellular matrix (ECM) mineralization and calcium deposition in vitro [43, 44].

Conclusion

Silicon substitute HA powders were successfully prepared by a sol-gel method and fully characterized to confirm the incorporation of Si into HA structure. Si-HA and HA were found to be non-cytotoxic as they did not have a significant effect on the growth pattern of the cells. In fact, particles were found to positively influence osteogenic differentiation of ADSCs in vitro. Overall, results from this study suggest that Si-HA particles have the potential to be applied for a range of bone regenerative applications in the form of particulate, fillers, coatings, and scaffolds.

References

1. Olszta MJ, Cheng X, Jee SS, Kumar R, Kim Y-Y, Kaufman MJ, et al. Bone structure and formation: a new perspective. Materials Science and Engineering: R: Reports. 2007;58:77–116.
2. Sobczak-Kupiec A, Pluta K, Drabczyk A, Włoś M, Tyliszczak B. Synthesis and characterization of ceramic-polymer composites containing bioactive synthetic hydroxyapatite for biomedical applications. Ceram Int. 2018;44:13630–8.
3. Kolmas J, Krukowski S, Laskus A, Jurkitewicz M. Synthetic hydroxyapatite in pharmaceutical applications. Ceram Int. 2016;42:2472–87.

4. Tracy BM, Doremus R. Direct electron microscopy studies of the bone—hydroxylapatite interface. J Biomed Mater Res. 1984;18: 719–26.
5. Hellmich C, Ulm F-J. Average hydroxyapatite concentration is uniform in the extracollagenous ultrastructure of mineralized tissues: evidence at the 1–10-μm scale. Biomech Model Mechanobiol. 2003;2:21–36.
6. Weiner S, Wagner HD. The material bone: structure-mechanical function relations. Annu Rev Mater Sci. 1998;28:271–98.
7. Poinern GE, Brundavanam RK, Mondinos N, Jiang Z-T. Synthesis and characterisation of nanohydroxyapatite using an ultrasound assisted method. Ultrason Sonochem. 2009;16:469–74.
8. De Bruijn J, Van Blitterswijk C, Davies J. Initial bone matrix formation at the hydroxyapatite interface in vivo. J Biomed Mater Res. 1995;29:89–99.
9. Radin S, Ducheyne P. The effect of calcium phosphate ceramic composition and structure on in vitro behavior. II. Precipitation. J Biomed Mater Res. 1993;27:35–45.
10. Patel N, Best S, Bonfield W, Gibson IR, Hing K, Damien E, et al. A comparative study on the in vivo behavior of hydroxyapatite and silicon substituted hydroxyapatite granules. J Mater Sci Mater Med. 2002;13:1199–206.
11. Höland W, Vogel W, Naumann K, Gummel J. Interface reactions between machinable bioactive glass-ceramics and bone. J Biomed Mater Res. 1985;19:303–12.
12. Webster TJ, Ergun C, Doremus RH, Bizios R. Hydroxylapatite with substituted magnesium, zinc, cadmium, and yttrium. II. Mechanisms of osteoblast adhesion. J Biomed Mater Res. 2002;59:312–7.
13. Hutmacher DW, Schantz JT, Lam CXF, Tan KC, Lim TC. State of the art and future directions of scaffold-based bone engineering from a biomaterials perspective. J Tissue Eng Regen Med. 2007;1:245–60.
14. Gibson I, Best S, Bonfield W. Chemical characterization of silicon-substituted hydroxyapatite. J Biomed Mater Res. 1999;44:422–8.
15. Carlisle EM. Silicon: a possible factor in bone calcification. Science. 1970;167:279–80.
16. El Yacoubi A, Massit A, Fathi M, El Idrissi BC, Yamni K. Characterization of silicon-substituted hydroxyapatite powders synthesized by a wet precipitation method. IOSR J Appl Chem. 2014;7:24–9.
17. Moheet IA, Luddin N, Ab Rahman I, Kannan TP, Ghani NRNA. Evaluation of mechanical properties and bond strength of nano-hydroxyapatite-silica added glass ionomer cement. Ceram Int. 2018;44:9899–906.
18. Hijón N, Cabanas MV, Pena J, Vallet-Regí M. Dip coated silicon-substituted hydroxyapatite films. Acta Biomater. 2006;2(2):567–74.
19. Latifi S, Fathi M, Golozar M. Preparation and characterisation of bioactive hydroxyapatite–silica composite nanopowders via sol–gel method for medical applications. Adv Appl Ceram. 2011;110:8–14.
20. Kim HW, Kim HE, Salih V, Knowles JC. Hydroxyapatite and titania sol–gel composite coatings on titanium for hard tissue implants; mechanical and in vitro biological performance. J Biomed Mater Res B. 2005;72:1–8.
21. Andersson J, Areva S, Spliethoff B, Lindén M. Sol–gel synthesis of a multifunctional, hierarchically porous silica/apatite composite. Biomaterials. 2005;26:6827–35.
22. Malakauskaite-Petruleviciene M, Stankeviciute Z, Niaura G, Prichodko A, Kareiva A. Synthesis and characterization of sol–gel derived calcium hydroxyapatite thin films spin-coated on silicon substrate. Ceram Int. 2015;41:7421–8.
23. Zuk PA, Zhu M, Ashjian P, De Ugarte DA, Huang JI, Mizuno H, et al. Human adipose tissue is a source of multipotent stem cells. Mol Biol Cell. 2002;13:4279–95.
24. Alabdulkarim Y, Ghalimah B, Al-Otaibi M, Al-Jallad HF, Mekhael M, Willie B, et al. Recent advances in bone regeneration: the role of adipose tissue-derived stromal vascular fraction and mesenchymal stem cells. J Limb Lengthen Reconstr. 2017;3:4.
25. Reumann MK, Linnemann C, Aspera-Werz RH, Arnold S, Held M, Seeliger C, et al. Donor site location is critical for proliferation, stem cell capacity, and osteogenic differentiation of adipose mesenchymal stem/stromal cells: implications for bone tissue engineering. Int J Mol Sci. 2018;19.
26. Beigi MH, Atefi A, Ghanaei HR, Labbaf S, Ejeian F, Nasr-Esfahani MH. Activated platelet-rich plasma improves cartilage regeneration using adipose stem cells encapsulated in a 3D alginate scaffold. J Tissue Eng Regen Med. 2018;12:1327–38.
27. Milner DJ, Bionaz M, Monaco E, Cameron JA, Wheeler MB. Myogenic potential of mesenchymal stem cells isolated from porcine adipose tissue. Cell Tissue Res. 2018;372:507–22.
28. Wang Y-H, Wu J-Y, Kong SC, Chiang M-H, Ho M-L, Yeh M-L, et al. Low power laser irradiation and human adipose-derived stem cell treatments promote bone regeneration in critical-sized calvarial defects in rats. PLoS One. 2018;13:e0195337.
29. Houreh AB, Labbaf S, Ting H-K, Ejeian F, Jones JR, Esfahani M-HN. Influence of calcium and phosphorus release from bioactive glasses on viability and differentiation of dental pulp stem cells. J Mater Sci. 2017;52:8928–41.
30. Gholami S, Labbaf S, Houreh AB, Ting H-K, Jones JR, Esfahani M-HN. Long term effects of bioactive glass particulates on dental pulp stem cells in vitro. Biomedical Glasses. 2017;3:96–103.
31. Miron R, Hedbom E, Saulacic N, Zhang Y, Sculean A, Bosshardt D, et al. Osteogenic potential of autogenous bone grafts harvested with four different surgical techniques. J Dent Res. 2011;90:1428–33.
32. Porter AE, Patel N, Skepper JN, Best SM, Bonfield W. Effect of sintered silicate-substituted hydroxyapatite on remodelling processes at the bone–implant interface. Biomaterials. 2004;25:3303–14.
33. Bang L, Long B, Othman R. Carbonate hydroxyapatite and silicon-substituted carbonate hydroxyapatite: synthesis, mechanical properties, and solubility evaluations. Sci World J. 2014:2014.
34. Porter AE, Botelho CM, Lopes MA, Santos JD, Best SM, Bonfield W. Ultrastructural comparison of dissolution and apatite precipitation on hydroxyapatite and silicon-substituted hydroxyapatite in vitro and in vivo. J Biomed Mater Res A. 2004;69:670–9.
35. Bianco A, Cacciotti I, Lombardi M, Montanaro L. Si-substituted hydroxyapatite nanopowders: synthesis, thermal stability and sinterability. Mater Res Bull. 2009;44:345–54.
36. Arcos D, Rodríguez-Carvajal J, Vallet-Regí M. The effect of the silicon incorporation on the hydroxylapatite structure. A neutron diffraction study. Solid State Sci. 2004;6:987–94.
37. Zheng Y, Dong G, Deng C. Effect of silicon content on the surface morphology of silicon-substituted hydroxyapatite bio-ceramics treated by a hydrothermal vapor method. Ceram Int. 2014;40: 14661–7.
38. Aminian A, Solati-Hashjin M, Samadikuchaksaraei A, Bakhshi F, Gorjipour F, Farzadi A, et al. Synthesis of silicon-substituted hydroxyapatite by a hydrothermal method with two different phosphorous sources. Ceram Int. 2011;37:1219–29.
39. Dong G, He L, Pang D, Wei L, Deng C. An in situ study of the deposition of a calcium phosphate mineralized layer on a silicon-substituted hydroxyapatite sensor modulated by bovine serum albumin using QCM-D technology. Ceram Int. 2016;42:18648–56.

40. Bang L, Ishikawa K, Othman R. Effect of silicon and heat-treatment temperature on the morphology and mechanical properties of silicon-substituted hydroxyapatite. Ceram Int. 2011;37:3637–42.
41. Porter AE. Nanoscale characterization of the interface between bone and hydroxyapatite implants and the effect of silicon on bone apposition. Micron. 2006;37:681–8.
42. Porter AE, Best SM, Bonfield W. Ultrastructural comparison of hydroxyapatite and silicon-substituted hydroxyapatite for biomedical applications. Biomed Mater Res A. 2004;68:133–41.
43. Maeno S, Niki Y, Matsumoto H, Morioka H, Yatabe T, Funayama A, et al. The effect of calcium ion concentration on osteoblast viability, proliferation and differentiation in monolayer and 3D culture. Biomaterials. 2005;26:4847–55.
44. Marie PJ. The calcium-sensing receptor in bone cells: a potential therapeutic target in osteoporosis. Bone. 2010;46:571–6.